Λ Doublet Propensities in Ar−NO Rotationally Inelastic Scattering at 220 meV

Ao Lin, Stiliana Antonova,[†] Antonis P. Tsakotellis, and George C. McBane*

Department of Chemistry, The Ohio State University, Columbus, Ohio 43210

Received: October 22, 1998; In Final Form: January 3, 1999

Collisions between argon and nitric oxide were studied in crossed supersonic beams. Resonance-enhanced multiphoton ionization was used to determine postcollision relative densities of many rotational, spin−orbit, and Λ doublet states. A double-beam reference technique was used to compensate for possible saturation in the REMPI probe. A preference for the production of the Π(*A″*) Λ doublet component was observed in both final spin−orbit states. Quantum scattering calculations on the potential surfaces of Alexander (*J. Chem. Phys.* **1993**, *99*, 7725) agree well with the Λ doublet propensity but underestimate the observed probability for spin−orbit-changing collisions.

1. Introduction

Inelastic collisions of a diatomic molecule in a Π electronic state with a structureless atom are among the simplest molecular events that are dependent on more than one Born−Oppenheimer potential energy surface. Nitric oxide is chemically stable and spectroscopically convenient and has been the target molecule of choice for experimental studies of $^2\Pi$ collision dynamics. Joswig et al. described the first laser-based crossed molecular beam studies of Ar−NO collisions in 1982 and 1986.[1,2] Those experiments were interpreted in terms of an electron-gas potential surface developed by Nielson, Parker, and Pack.[3] In the past six years, several experimental groups have returned to the study of rotationally inelastic rare gas−NO collisions. The new experimental data include state-to-state differential[4−7] and integral[7,8] cross sections and differential and integral alignment moments[7] for scattering out of the lowest rotational state of NO, parity-resolved integral cross sections for scattering from ground state,[9] vibrationally excited,[10] and oriented NO,[11] and state-to-state rate coefficients for ground and vibrationally excited NO at several different temperatures.[12−16]

Alexander, encouraged by some of the new experiments, constructed high-quality potential energy surfaces for the He−NO[17] and Ar−NO[18] systems and performed scattering calculations that predicted integral and differential cross sections for specific NO product states. His work has generated additional interest among experimentalists, including ourselves.

Alexander predicted[18] a propensity for formation of the Π-(*A″*) Λ doublet state in many rotational levels of the scattered products, even though the low-*J* precollision NO molecules have equal population in the two Λ doublet components. This propensity originates in interference among scattering "paths" on the two Ar−NO potential surfaces of *A′* and *A″* symmetry. It arises for final states of NO that have some Hund's case (b) character, that is, for which the molecular wave function is a mixture of $\Omega = {}^1/_2$ and $\Omega = {}^3/_2$ functions.

Experimental evidence for a Λ doublet propensity has so far been sparse. Bieler et al. saw indications of such a propensity but were cautious about their interpretation because of uncer-

tainty in the conversions of observed signal intensities to populations.[8] The experiments of van Leuken et al.[9] and of Drabbels et al.[10] probed transitions between cleanly prepared Λ doublet states but could not address the creation of unequal Λ doublet populations directly. Meyer's counterpropagating beam experiments on He−NO collisions did not detect preferential Λ doublet populations.[7] The predicted propensity does appear for a few final rotational levels in the state-to-state differential cross sections of Jons et al.[5,6]

In this paper we report measurements of relative state-to-state densities of scattered NO after collisions with Ar at 220 meV center of mass (COM) energy. Our experiments are very similar to those of Bieler et al.[8] and Joswig et al.[1,2] We crossed supersonic beams of Ar and NO and measured scattered densities of NO in their intersection volume with resonance-enhanced multiphoton ionization. We compare our experimental results with quantum scattering calculations done with the HIBRIDON program[19] on Alexander's Ar−NO potential surfaces.

We have paid particular attention to extraction of relative densities from the experimental signals, to obtain clear evidence for or against the production of unequal Λ doublet densities. To that end, we have developed a "double-beam" version of REMPI. The experiment uses a reference cell filled with NO at room temperature. Each laser pulse is split into two nearly identical beams; one is used for the REMPI experiment in the scattering chamber, and the other is sent into the reference cell. The ionization probability for an NO molecule in the cell should be the same as that for a molecule in the same internal state and same position in the laser focal volume in the scattering chamber. The relative population of each internal state in the cell is known, so the ion signal collected in the cell provides a shot-to-shot measure of the effectiveness of the laser pulses in producing NO ions. With that measure we can convert the REMPI signal intensities into relative densities without making assumptions about (or careful measurements of) the dependence of the intensities on laser pulse energy and spatial distribution.

2. Experiment

The experimental setup is shown in Figure 1. Two supersonic beams, one of neat Ar and the other containing NO seeded in a rare gas mixture, crossed in the source region of a Wiley−

† Present address: Physics Department, Bryn Mawr College, Bryn Mawr, PA 19010.

* Corresponding author.

Λ Doublet Propensities in Ar−NO Scattering
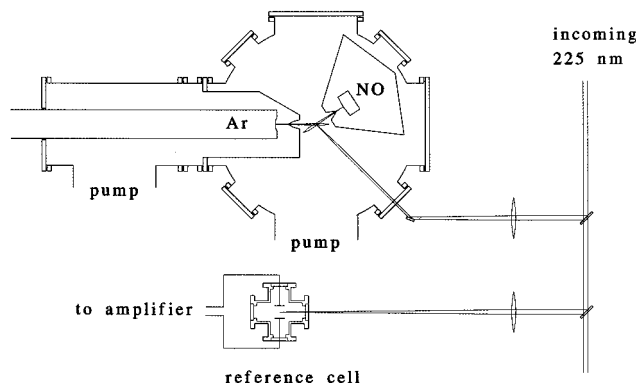
J. Phys. Chem. A, Vol. 103, No. 9, 1999 **1199**

Figure 1. Apparatus. The NO source chamber is evacuated by a pump behind the plane of the page; the ion flight tube extends out of the page. The ion optics are not shown.

McLaren mass spectrometer. Scattered NO molecules were state-selectively ionized with (1+1) REMPI through the NO $A^2\Sigma^+$ state.

A fast pulsed valve (R. M. Jordan) generated a supersonic jet of neat Ar from a source pressure of 6.4 bar with a pulse duration of about 75 μs. A rectangular skimmer made from two sharp steel blades mounted on a plate in the scattering chamber extracted a wedge-shaped beam with a divergence angle of 3.2° in the plane containing the NO and laser beams. The total distance from nozzle to beam intersection point was 115 mm.

The pulsed valve containing the NO mixture (7% NO, 15% Ar, 78% He) was the type designed by Proch and Trickl[20] and was mounted in a differentially pumped chamber. The mixture expanded from a stagnation pressure of 3.7 bar and passed through a 1.5 mm diameter skimmer (Beam Dynamics) 25 mm from the valve. The distance from the nozzle to the beam intersection point was 79 mm, and the pulse duration was approximately 170 μs. The NO and Ar beams intersected at 150° to give a center-of-mass collision energy of 1780 cm^{-1} with an energy spread of about 6.5%.

A dye laser (Continuum) pumped by an injection-seeded, Q-switched Nd:YAG laser (Spectra-Physics/Larry Wolford Services) provided the probe light. The dye laser used Rhodamine 6G Chloride dye (Exciton) dissolved in water. The dye laser beam was doubled and then mixed with 1064 nm light in a Spectra-Physics WEX, and the 225 nm output was separated from the other wavelengths in a four-prism filter so the beam did not "walk" as the wavelength was changed.

Two uncoated fused silica plates were inserted into the laser beam at 45° and produced two nearly identical reflected beams. A 1 m lens focused one of these beams into the scattering chamber, where it traveled in the same plane as the two gas beams at 135° from the Ar beam. The laser beam, linearly polarized in the plane of the molecular beams, crossed them in their intersection volume. Ions formed at the intersection were accelerated into the mass spectrometer flight tube and detected with a channel electron multiplier (DeTech). A fast preamplifier (Comlinear) amplified the detector output, and its output entered a gated integrator (SRS).

An identical lens focused the second reflected beam into a small cell containing approximately 0.1 Torr of a 1% NO/99% Ar mixture. Two 10 mm diameter disk-shaped electrodes, biased at +1 V and −1 V, collected the ions and electrons formed by the laser pulse. The electrode currents were amplified by a differential amplifier like that described by Adams et al.;[21] its output was integrated by a Princeton Applied Research boxcar integrator. Pressures were measured by a sensitive Bourdon gauge and a thermocouple gauge.

The laser and NO valve operated at 10 Hz. The Ar valve fired in a two shots on/two shots off pattern to permit correction for the background population of each rotational state in the unscattered molecular beam. (We used the 2/2 pattern because we found that the SRS 250 gated integrator inserted a small error into each sample that alternated in sign with each shot.) The data were collected in many overlapping sections of 0.75 nm each in the visible, each requiring about 10 min of laboratory time. REMPI signals from the cell and the electron multiplier were collected for eight laser shots (four with Ar and four without) at each laser wavelength. The laser wavelength was scanned with 0.001 nm steps (in the visible) over nearly the entire (0,0) band of the $A \leftarrow X$ transition during the data collection.

REMPI spectra of the unscattered NO beam showed that most of the NO molecules were well cooled; the fraction of the molecules in the lowest rotational level was 80 ± 10%. However, a small residual population of high rotational states remained in the beam. This population was much smaller than the scattered population for all rotational levels above $J = 9\frac{1}{2}$ in the lower spin−orbit state and for all the lines of the upper spin−orbit state. The data treatment procedures described below assume that scattering out of any final state is insignificant compared to scattering from the very low J populations into that state.

3. Data Analysis and Results

3.1. Reference Cell Conditions. For the reference cell signal to be useful, the ion signal collected by the electrodes should be proportional to the total number of ions formed in the volume between the electrodes. The proportionality constant must be independent of the laser pulse intensity and independent of the particular internal state of NO being probed. Several different processes can destroy the proportionality if they are not controlled.

First, the density of NO must be kept low enough that no appreciable absorption of the laser beam occurs in the cell. If the density is too high, the light intensity between the electrodes will be lower when the laser is tuned to a wavelength with strong NO absorption. We monitored absorption by placing a quartz cuvette filled with Rhodamine 6G dye at the cell output window and detecting fluorescence from the dye with a photodiode.

Second, collisions between molecules in the cell must not alter the ionization probabilities. At 100 mTorr, the rough gas-kinetic collision time is 1 μs, much longer than the 8 ns laser pulse. Therefore we do not expect collisional perturbation effects to affect our analysis.

Third, secondary (avalanche) ionization in the reference cell should be avoided. Above a threshold electric field strength, electrons formed by REMPI and accelerated in the electric field of the collection electrodes can gain enough kinetic energy to ionize other NO molecules in collisions. The charged-particle gain in such secondary ionization is strongly dependent both on the ratio of electric field strength to gas density, E/n, and on the number of ions initially formed in the pulse. We eliminated this problem by using an electrode bias well below the ionization potential of NO, so that no secondary ions could be formed.

Finally, if the electrons and ions are not separated quickly enough in the electric field, they can recombine. Therefore, E/n should be large enough that ion−electron recombination events in the ionization volume are negligible. We found a compromise between low signal levels and recombination empirically, by recording the ion signal as a function of gas pressure in the cell. Figure 2 shows the observed charge as a function of
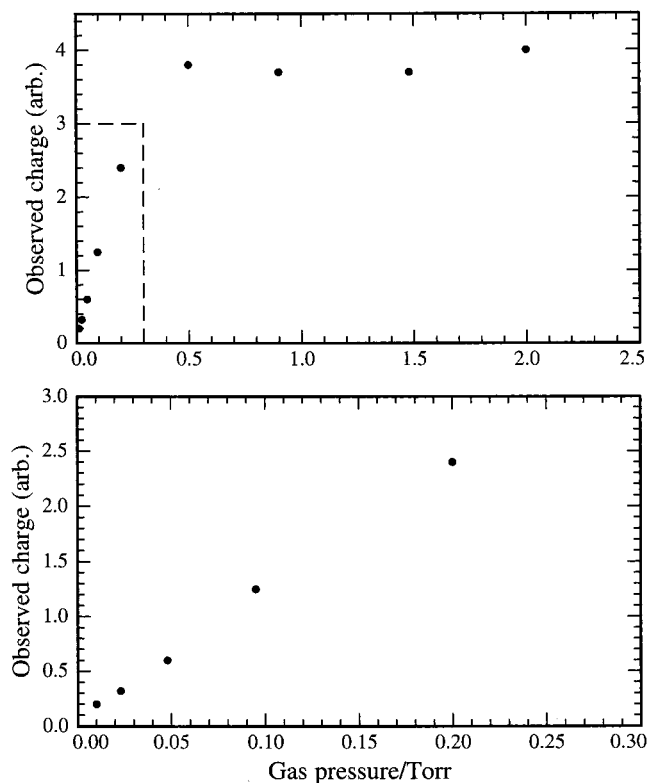
Figure 2. REMPI signal in reference cell as a function of gas (1% NO in Ar) pressure. The lower panel shows the five points at lowest pressure on an expanded pressure scale.

pressure in the cell. The signal on a single transition increased linearly with added gas until a threshold pressure was reached, above which it was nearly constant. We performed all the experiments with a cell pressure between 0.1 and 0.2 Torr, where the observed charge was linear with the cell pressure.

3.2. Determination of Densities. The ionization probability for a particular NO molecule during a particular laser pulse depends on the distribution of wavelengths in the pulse and on the intensity of the pulse as a function of time at the molecule's position. The dependence may be complicated and may be different for each internal state of NO. Our aim in developing the reference cell technique was to arrange that the ionization probability for a molecule in the cell on each laser pulse was equal to that for a corresponding molecule produced in an Ar–NO collision. We therefore tried to make the laser pulses going into the cell and the scattering chamber as similar as possible. We also tried to match the ion collection volumes and their locations with respect to the beam focus.

It is easy to imagine cases with unequal ionization probabilities in the cell and scattering chamber even under these conditions. For example, if the beam collisions produced products with a very strong alignment of angular momentum vectors, the product interactions with polarized laser light would not be well mimicked by those of the thermal molecules in the cell. Similarly, products with very high laboratory speeds and correspondingly large Doppler shifts would absorb at wavelengths different than that of the thermal sample.

A more subtle error could be introduced by the structure of longitudinal modes of the laser cavity. Our laser produces about seven modes in the UV with roughly a 1 GHz spacing. If the Doppler profiles of the cell and scattering chamber samples are not the same, and either of them is small compared to the laser mode spacing, it might be possible for the absorption profile of one sample to fall between longitudinal modes on a single laser

shot while the other absorbs strongly. The saturation behavior of the two would then not be similar, and one of the main advantages of the reference cell technique would be lost. In our experiment, this problem would be important if the differential cross section for production of any final state was very sharply peaked at one scattering angle; its Doppler profile might then be quite narrow. Neither the earlier experimental measurements of differential cross sections[4–6] nor our calculations (reported below) indicate that we should expect narrow speed distributions in the scattered NO. The calculated cell and scattering chamber Doppler widths are both 2–3 GHz.

We believe that these alignment and line shape effects introduce only small errors into our data analysis and have not tried to correct for them. However, future users of the technique may need to do so. The simple application given here assumes that the cell and chamber line shapes are the same. In our experiment both are dominated by the laser line width (mode envelope) and slight power broadening.

If we have succeeded in arranging that the ionization probabilities on individual shots are the same for the cell sample and the scattered molecules, then the signal intensities on a single laser pulse are

$$I_{cell} = G_{cell} \sum_{J,F_i,\epsilon} n_{cell}(JF_i\epsilon) \, P_I(JF_i\epsilon) \tag{1}$$

$$I_{SC} = G_{SC} \sum_{J,F_i,\epsilon} n_{SC}(JF_i\epsilon) \, P_I(JF_i\epsilon) \tag{2}$$

where the G terms represent the gain factors from number of ions produced to signal intensity in the cell and the scattering chamber, the n terms represent the densities of molecules in particular internal states in the detection volumes, and the P_I term is the ionization probability described above and is equal for a given internal state in both equations. The Λ doublet parity index ϵ is -1 for f and 1 for e states; in the F_1 spin–orbit state ($\Omega = 1/2$ in the case (a), low J limit), e corresponds to $\Pi(A')$ and f corresponds to $\Pi(A'')$, while in F_2 ($\Omega = 3/2$) e is $\Pi(A'')$ and f is $\Pi(A')$.[22]

If the rotational lines are well separated, the sum at a particular wavelength collapses to a single term:

$$I_{SC} = G_{SC} n_{SC}(JF_i\epsilon) \, P_I(JF_i\epsilon) \tag{3}$$

and similarly for the cell.

All the dependence on characteristics of a single laser pulse (wavelength, line width, spatial distribution of intensity) is contained in the P_I term. The most straightforward use of the cell signal is by shot-to-shot normalization:

$$n_{SC}(JF_i\epsilon) = \left(\frac{G_{cell}}{G_{SC}}\right)\left(\frac{I_{SC}}{I_{cell}}\right) n_{cell}(JF_i\epsilon) \tag{4}$$

All the terms on the right side of eq 4 are known except the gain factors, and their ratio is independent of internal state and laser intensity. (It should be possible to determine the ratio of gain factors in a calibration experiment and then make absolute determinations of scattered densities.) If eq 4 is applied to every laser shot that produced nonzero intensity in the reference cell, the results averaged appropriately, and the Ar-off background density subtracted, the result is

$$\Delta n_{SC}(JF_i\epsilon) = n_{cell}(JF_i\epsilon) \sum_{\lambda=\lambda_{min}}^{\lambda_{max}} \left[\left\langle\frac{I_{SC}(\lambda)}{I_{cell}(\lambda)}\right\rangle_{on} - \left\langle\frac{I_{SC}(\lambda)}{I_{cell}(\lambda)}\right\rangle_{off}\right] \tag{5}$$

Λ Doublet Propensities in Ar−NO Scattering

J. Phys. Chem. A, Vol. 103, No. 9, 1999 **1201**

This shot-to-shot normalization gave reasonable results for our experiment. However, the unaveraged cell-signal intensity in the denominators, especially near the edges of rotational lines, makes the procedure sensitive to noise in the reference signal. We therefore decided to calculate overall signal strengths, $\langle I_{cell} \rangle$ and $\langle I_{SC} \rangle$, across each rotational line and use the ratios of those averaged quantities to evaluate densities. For each isolated line, we chose a set of upper and lower limit wavelengths λ_{min} and λ_{max} that enclosed the entire line in all three spectra. We then estimated the scattered relative density with the expression

$$\Delta n_{SC}(JF_i\epsilon) = n_{cell}(JF_i\epsilon) \frac{\displaystyle\sum_{\lambda=\lambda_{min}}^{\lambda_{max}} [\langle I_{SC}(\lambda)\rangle_{on} - \langle I_{SC}(\lambda)\rangle_{off}]}{\displaystyle\sum_{\lambda=\lambda_{min}}^{\lambda_{max}} \langle I_{cell}(\lambda)\rangle_{on+off}} \quad (6)$$

In eq 6, $n_{cell}(JF_i\epsilon)$ represents the Boltzmann fractional population of the $(JF_i\epsilon)$ level at the 295 K temperature of the reference cell, $\langle I_{SC}(\lambda)\rangle_{on}$ represents the average of the four scattering chamber signals at wavelength λ taken with the Ar beam on, and similar definitions hold for $\langle I_{SC}(\lambda)\rangle_{off}$ and $\langle I_{cell}(\lambda)\rangle_{on+off}$. In the last case the reference cell signals from all eight laser shots are averaged. We found scaling factors between the different sections by comparing relative densities calculated from common lines.

Equation 6 is a good approximation to eq 5 if the shot-to-shot variations in the ionization probabilities are small. We checked the accuracy of eq 6 in two ways. First, we measured the population distribution of a thermal NO sample in the scattering chamber and found that the temperature we extracted was accurate. Second, we used Monte Carlo simulation. The Monte Carlo program produced simulated data files with known rotational and Λ-doublet distributions and noise characteristics very similar to those of the experiment. We subjected many simulated data sets to analysis with eq 6 and found that it reproduced the correct distributions reliably.

Data from one experimental scan are shown in Figure 3. The top panel shows $\langle I_{SC}(\lambda)\rangle_{on}$ and $\langle I_{SC}(\lambda)\rangle_{off}$ separately, the middle panel shows $\langle I_{SC}(\lambda)\rangle_{on} - \langle I_{SC}(\lambda)\rangle_{off}$, and the bottom panel shows $\langle I_{SC}(\lambda)\rangle_{on+off}$.

3.3. Results. Each of the $(JF_i\epsilon)$ states is probed by rotational lines from two branches.[22] Q_{11}/P_{21} and R_{21}, for example, are transitions from the same (JF_1f) state to different rotational states of the $A^2\Sigma^+$ state. The relative densities derived from the two branches should agree if alignment effects are not important; we checked for a tendency for one of the two branches to give higher apparent densities than the other and did not find one.

Figure 4 shows the relative densities produced by eq 6. $n_{cell}(JF_i\epsilon)$ is a constant for each line, so the random error in n_{SC} arises from accumulation of random errors in the shot-to-shot intensities. We calculated the standard errors $\sigma_{on}(\lambda)$, $\sigma_{off}(\lambda)$, and $\sigma_{cell}(\lambda)$ from fluctuations in the intensities and then propagated them through eq 6 to get the error bars displayed in Figure 4. The error bars on individual points therefore indicate the random error associated with statistical fluctuations within a single measured rotational line. Several measurements were performed for most final states; we have plotted the results individually to convey their reproducibility. In most cases, the reproducibility error is larger than the statistical error in a single experiment.

3.4. Errors. Our choices of the wavelength limits of each line, λ_{min} and λ_{max}, do affect the extracted densities slightly.
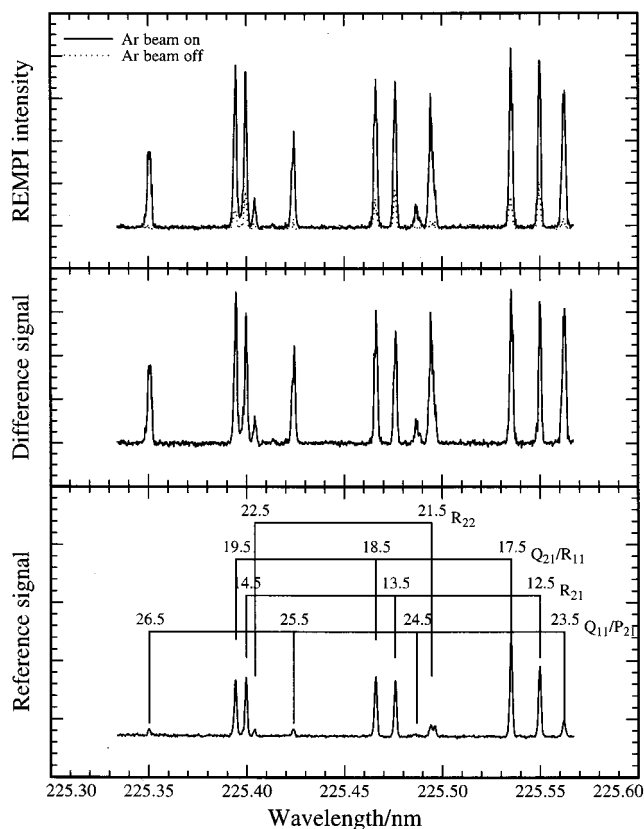

Figure 3. Spectra from the scattering chamber and reference cell for one section of the (0,0) band.

The Monte Carlo simulation showed that these errors were always less than 10% of the density and generally smaller than the statistical errors already considered.

Angular momentum anisotropy (alignment) in the postcollision population could introduce errors in the measured densities, since we used only a single laser polarization.[23] The semiclassical argument of Alexander and Dagdigian[24] suggests that alignment effects should be small in our experiment, where impulsive collisions dominated by short-range interactions are most important. On the other hand, Meyer[7] did observe negative alignment (tendency for $|M| \approx 0$ when the z axis is along the initial relative velocity) in his similar experiment on He−NO collisions. A classical, high-J analysis indicates that negative alignment should enhance the intensities of pure R or P lines compared to mixed Q/P and Q/R lines for our experimental geometry. We did not observe such a trend. We cannot rule out the presence of alignment in our experiment, but we believe that its magnitude is small enough and our experiment is insensitive enough to its effects that it does not introduce a significant systematic error.

The density of a particular final state of NO will not be uniform throughout the molecular beam intersection volume, and the dependence of density on position will not be the same for all the final states. Therefore different positions of the probe laser might result in different measured density distributions. We discuss this effect (the density-to-flux transformation) more fully in the next section; we expect it to be fairly small. Nonetheless, changes in beam arrangments probably account for some of the spread between different measurements apparent in Figure 4.

3.5. Effects of Density-to-Flux Transformation. The relative densities shown in Figure 4 have not been subjected to a density-to-flux transformation,[25] so they are not directly comparable to
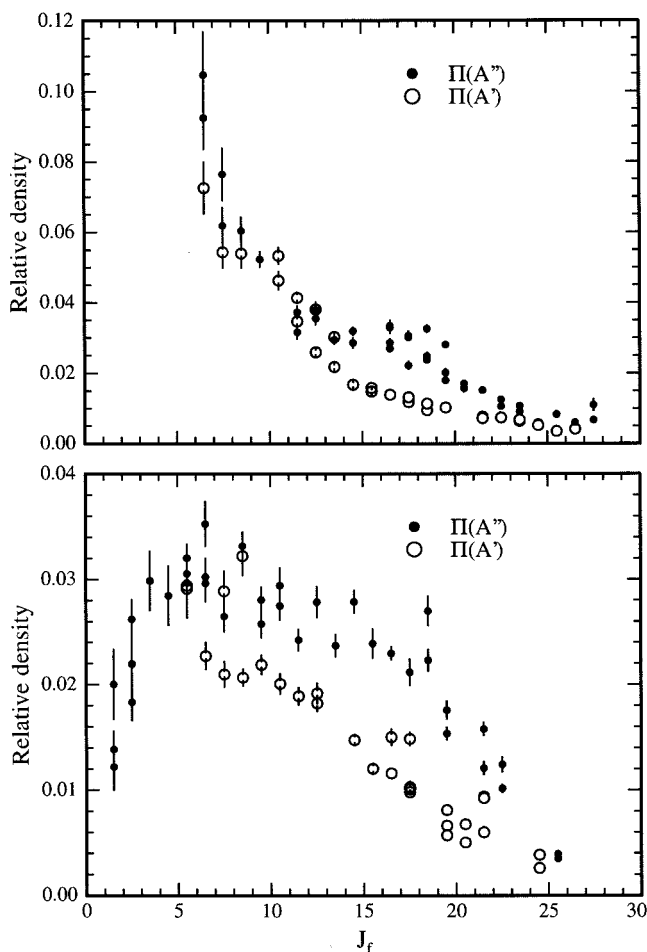
Figure 4. Observed relative densities for the $F_1 \rightarrow F_1$ (upper panel) and $F_1 \rightarrow F_2$ (lower panel) transitions. Filled circles indicate the Π-(A'') Λ doublet component, and open circles show $\Pi(A')$. The error bars represent statistical error in individual measurements; the scatter of points indicates the reproducibility of the results.

calculated cross sections. However, kinematics are sufficient to estimate the qualitative effects of the transformation in this case. The NO beam is fast in the laboratory frame, and the center of mass moves slowly because of the large intersection angle between the two beams. At low to moderate ΔJ, the laboratory speeds of products scattered into all angles are nearly equal. The density-to-flux transformation will therefore serve to enhance the sensitivity to larger ΔJ slightly, and at low to moderate ΔJ, a plot of integral cross sections will appear similar to the density plot but will fall off somewhat more steeply with J. At higher ΔJ, where the COM speed of a scattered NO molecule is comparable to the laboratory speed of the center of mass, the shape of the differential cross sections (DCS) will be more important.

We do not have complete calculated DCS available for our collision energy, because the HIBRIDON program discussed below does not yet support extraction of differential cross sections for coupled-states calculations. However, we obtained a "typical" set of DCS by carrying out model Ar−NO calculations with the MOLSCAT program.[26] MOLSCAT can treat only single-surface calculations, and we used the sum of the A' and A'' potential surfaces of Alexander as an "effective surface". This approximate calculation should describe the qualitative features of scattering within the lower spin−orbit manifold reasonably, though of course it cannot be expected to reflect interference effects between the two surfaces. We find

that integral cross sections from the single-surface calculation agree with the HIBRIDON calculations very well at high ΔJ, and match the qualitative falloff with ΔJ reasonably at low to moderate (<20) ΔJ, though they do not reproduce the interference oscillations well. The DCS from the model calculation have the expected trend from mostly forward scattering at low ΔJ to mostly backward at high ΔJ; between, they have complicated shapes with several maxima.

We used these crude DCS to evaluate the density-to-flux correction factors $\langle g/v_f \rangle$ as defined by Dagdigian,[27] where g is the initial relative speed, v_f is the final laboratory frame speed of the detected molecules, and the brackets denote an average over scattering angles weighted by the normalized differential cross section. Those calculations show that the experimental sensitivity is nearly constant for $5 \leq \Delta J \leq 15$ and increases slowly at higher ΔJ, becoming about 1.3 times larger than the low-ΔJ value at $\Delta J = 22$ and 1.6 times larger at $\Delta J = 28$. A more sophisticated evaluation of the correction factors, similar to the method of Naulin et al.[28] but extended to include arbitrary beam intersection angles and a Gaussian laser beam profile, gave similar results. Our qualitative conclusions above were thus confirmed; the main effect of the density-to-flux transformation is to enhance the experimental sensitivity modestly at high ΔJ.

4. Calculations

We performed quantum scattering calculations on the ab initio potential energy surfaces of Alexander,[18] both at our experimental collision energy of 1780 cm^{-1} and at 2250 cm^{-1} for comparison with the data of Bieler et al.[8] At the high collision energies of the experiments, full close-coupled calculations are impractical; we used the coupled states (CS) approximation of McGuire and Kouri.[29] The calculations were carried out with the HIBRIDON package.[19,30,31] All the open rotational levels and one closed level were included in the basis set. The partial wave sum was terminated at orbital angular momentum 275; all the integral cross sections for $\Delta J \geq 4$ were converged to four significant figures.

The coupled states approximation is best for impulsive collisions, so it should work better for a given collider pair as the collision energy increases. Alexander and co-workers have established its accuracy in He−NO collisions at energies above 600 cm^{-1}.[16,17] In addition, we performed Ar−NO CS calculations at 442 cm^{-1} for comparison with Alexander's converged close-coupled results.[18] At that energy, the e/f preserving and e/f changing cross sections, for both spin−orbit manifolds, were nearly identical to those Alexander obtained with exact calculations and reported in Figure 9 of his paper.[18] The only qualitative difference appeared in the integral cross sections for ΔJ of 1 or 2 in spin−orbit-changing collisions, where the parity-changing cross sections are larger in the CS than the CC results and the parity-conserving ones are lower. The absolute cross sections in the two calculations agreed to within better than 10% everywhere except for those two transitions. We concluded that at the energy of our experiments, about 4 times higher than this test calculation, the CS approximation should not introduce significant errors.

The results at our collision energy are plotted in Figure 5 as definite-symmetry cross sections, weighted for the 80%/20% initial populations of $J = 1/2$ and $3/2$ in the NO molecular beam. These cross sections are the sums of cross sections from the two initial Λ doublet states into final states of particular

Λ Doublet Propensities in Ar−NO Scattering
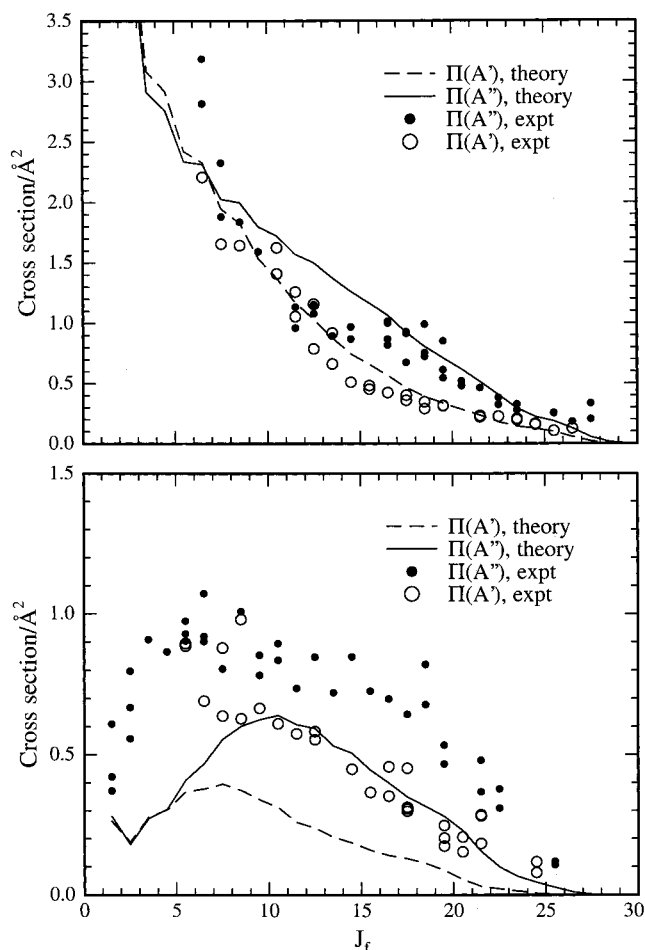
J. Phys. Chem. A, Vol. 103, No. 9, 1999 **1203**

Figure 5. Calculated cross sections and experimental densities for transitions into different final levels. The upper panel shows $F_1 \to F_1$ results; the lower panel shows $F_1 \to F_2$. The experimental data sets have been scaled to match the $F_1 \to F_1$ theoretical cross sections for $J > 7^1/_2$.

reflection symmetry:

$$\sigma_{\text{eff}}(JF_1A') = f_{1/2}\left[\sigma\left(\tfrac{1}{2}F_1e \to JF_1e\right) + \sigma\left(\tfrac{1}{2}F_1f \to JF_1e\right)\right] +$$
$$f_{3/2}\left[\sigma\left(\tfrac{3}{2}F_1e \to JF_1e\right) + \sigma\left(\tfrac{3}{2}F_1f \to JF_1e\right)\right] \quad (7)$$

$$\sigma_{\text{eff}}(JF_1A'') = f_{1/2}\left[\sigma\left(\tfrac{1}{2}F_1e \to JF_1f\right) + \sigma\left(\tfrac{1}{2}F_1f \to JF_1f\right)\right] +$$
$$f_{3/2}\left[\sigma\left(\tfrac{3}{2}F_1e \to JF_1f\right) + \sigma\left(\tfrac{3}{2}F_1f \to JF_1f\right)\right] \quad (8)$$

In eqs 7 and 8, $f_{1/2}$ and $f_{3/2}$ are the initial populations in the two lowest rotational levels. The definitions for $\sigma_{\text{eff}}(JF_2A')$ and $\sigma_{\text{eff}}(JF_2A'')$ are similar except the target levels are JF_2f for A' and JF_2e for A''. Since our experiments do not select the initial Λ doublet, but the postcollision Λ doublets are spectroscopically distinct, these definite-symmetry cross sections are the appropriate quantities for comparison. The experimental data from Figure 4 are also shown in the figure. The experiment measures only relative densities. The experimental results have been scaled to make the sum of $F_1 \to F_1$ densities for $J > 7^1/_2$ match the theoretical result.

5. Discussion

5.1. Λ Doublet Propensities. We observe a clear propensity for population of the $\Pi(A'')$ Λ doublet component for $J \geq 13^1/_2$

in F_1 and $J \geq 6^1/_2$ in F_2, confirming the earlier tentative observation of Bieler et al.[8] Roughly two-thirds of the total population appears in that component on some rotational lines. In both spin−orbit conserving and spin−orbit changing collisions, the propensity for production of the $\Pi(A'')$ component calculated from Alexander's potential energy surfaces agree very well with our observations. The calculated and observed propensities have one qualitative difference: in the $F_1 \to F_1$ experimental results, the propensity "turns on" between $J = 11^1/_2$ and $14^1/_2$, while in the calculation it appears more gradually beginning at about $J = 7^1/_2$.

The observed propensity must arise from interference among scattering paths on the A' and A'' potential surfaces, but a simple qualitative explanation of the $\Pi(A'')$ preference is not obvious. For scattering of a pure Hund's case (a) molecule in the energy sudden approximation, no propensity is expected in an experiment that begins with equal initial population of the Λ doublet components.[32] In scattering of a π^1 mixed case molecule like NO, Dagdigian et al. predicted a $\Pi(A'')$ propensity for direct (e.g., Born approximation) scattering.[33] However, their argument should not apply to our experiment, since NO is a good case (a) molecule for low J, and Alexander's Ar−NO potential has no terms capable of direct coupling between the ground state and states with $J \geq 10^1/_2$.[18] The transition from case (a) to intermediate case coupling—that is, mixing of the two definite-Ω case (a) basis functions as J increases—is clearly required for the observed Λ doublet propensity, but we have no clear rationale for choosing whether the $\Pi(A')$ or the $\Pi(A'')$ state will be preferentially populated. Thus we may either regard the $\Pi(A'')$ propensity as a numerical accident arising from the details of the two Ar−NO potential surfaces or conclude that the propensity rule of Dagdigian et al. has wider applicability than its authors claimed.

Kovalenko and Delos recently described a semiclassical model of Λ doublet transitions in diatomic molecules.[34] They have so far addressed only singlet states. Because the propensity for $\Pi(A'')$ we observe is closely related to the transition from Hund's case (a) to intermediate case coupling, the influence of spin is crucial. The analysis of Kovalenko and Delos is therefore not yet applicable to our experiment. We are optimistic that extensions of their work to a more realistic NO model will provide satisfying physical insights into the observed propensity.

5.2. Rotational Distributions. The overall shapes of the rotational distributions agree well with the calculations and with the observations at higher collision energy of Bieler et al. The densities fall off monotonically for $J > 7^1/_2$ in the lower spin−orbit state; our data do not determine the densities at lower J well because of uncertainties in the subtraction of background density in the unscattered beam. (Errors in the background subtraction may account for the discrepancy at $J = 6^1/_2$ in the $F_1 \to F_1$ results.)

In the $F_1 \to F_2$ transitions, the $\Pi(A'')$ densities rise at low J and go through a maximum near $J = 6^1/_2$. The calculated cross sections do not reach their maximum until $J = 10^1/_2$. The same discrepancy appears when our CS results at 2250 cm^{-1} are compared with the data of Bieler et al.; the experimental results show a maximum at $J = 7^1/_2$, while the calculated cross sections are again largest at $J = 10^1/_2$. Neither experimental group corrected the observed densities for a density-to-flux transformation, so it is possible that the discrepancy is artifactual, but in light of our earlier discussion we think that is unlikely. The point could be resolved with accurate calculated differential cross sections.

The maximum in the $F_1 \rightarrow F_2$, $\Pi(A')$ distribution is not well determined in either set of experiments because of spectral congestion at low J. The calculated $\Pi(A')$ cross sections have maxima at $J = 7^{1}/_{2}$ for both energies.

5.3. Spin−Orbit Ratio. The most obvious discrepancy between the theoretical and experimental results is the fraction of collision events that produce $F_1 \rightarrow F_2$ transitions. In Figure 5, the $F_1 \rightarrow F_1$ and $F_1 \rightarrow F_2$ experimental results have been scaled by the same factor, to make the sum of the $F_1 \rightarrow F_1$, $J \geq 7^{1}/_{2}$ experimental densities match the theoretical result. The sum of the $F_1 \rightarrow F_2$ experimental densities is then 1.8 times larger than the corresponding theoretical sum. That is, we observe nearly twice as much $F_1 \rightarrow F_2$ scattering as the calculations predict.

In view of the otherwise very good agreement between experiment and theory, the factor of 2 discrepancy surprised us. It is not likely that the CS approximation in the scattering calculations is contributing such a large error. The discrepancy must be caused by errors in the Ar−NO potential surfaces, or errors in the experiment or its interpretation. We believe the experiment itself is consistent and reliable; checks of intensity ratios between close-lying F_1 and F_2 rotational lines, measured in separate experimental campaigns several months apart, gave results within a few percent of one another. However, at least two effects we ignored in the data analysis might be contributing: the density-to-flux transformation and possible angular momentum alignment.

Since the internal energy of an NO molecule is always higher in F_2 than in F_1 for the same J, the center-of-mass speeds for molecules scattered into F_2 will be lower. If those molecules are on average slower in the lab frame, the experiment will be more sensitive to them and the apparent amount of $F_1 \rightarrow F_2$ scattering will increase. We have estimated the importance of this effect with the crude differential cross sections discussed above, under the additional assumption that the differential cross section for production of a given final J is the same for $F_1 \rightarrow F_1$ and $F_1 \rightarrow F_2$ transitions. In that case, the increase in sensitivity for F_2 is about 4% at low J, rises slowly to 10% at $J = 25^{1}/_{2}$, and finally becomes about 25% at the highest energetically accessible rotational levels. We therefore expect an overall effect of perhaps 7%. Variations in differential cross sections for the spin−orbit conserving and spin−orbit changing collisions will modify these results, but it is unlikely that realistic differential cross sections will account for the entire discrepancy through the density-to-flux transformation.

Strong angular momentum alignment in the scattered molecules would also introduce errors. Our results for the $\Pi(A'')$ Λ doublet components come from both main and satellite branches, so there is no simple prediction for their response to alignment. However, the $\Pi(A')$ results in F_1 come mainly from Q_{21}/R_{11} lines, and the $\Pi(A')$ results in F_2 come mainly from Q_{12}/P_{22} lines. These two branches should have the same response to angular momentum alignment. Therefore, for alignment to be the cause of our spin−orbit discrepancy, the alignment in the molecules scattered into F_1 would have to be substantially different from that in F_2.

Several earlier measurements have also addressed the ratio of spin−orbit changing to spin−orbit conserving collisions. Bieler et al. determined spin−orbit ratios at 500 and 2250 cm^{-1}. Our CS calculations at the higher energy give a spin−orbit ratio that is smaller by a factor of 1.2 than their result. Alexander compared accurate CC calculations with the 442 cm^{-1} results of Joswig et al.[2] in his report of the Ar−NO potential surfaces;[18] there, the calculations appeared to underestimate the $F_1 \rightarrow F_2$

cross sections by roughly a factor of 2. The comparison is not clear-cut, however, because it is not clear which Λ doublet component was probed in the experiment. Finally, Drabbels et al.[10] measured spin−orbit changing cross sections in scattering of vibrationally excited NO from He. Calculations on a He−NO surface (obtained by methods similar to those for the Ar−NO surface considered here) again underestimated the probability of $F_1 \rightarrow F_2$ transitions by about a factor of 2. In light of this consistent evidence, we conclude that errors in the potential surface are contributing to the disagreement between theory and experiment.

6. Conclusions

NO molecules scattered from Ar at 1780 cm^{-1} preferentially occupy the $\Pi(A'')$ Λ doublet levels. The propensity is accurately predicted by coupled-states calculations on the ab initio potential surfaces of Alexander.[18] The shapes of the postcollision rotational distributions are also fairly well predicted, though there is a small disagreement over the position of the maximum in the rotational distribtion for spin−orbit changing collisions. The calculations disagree with the experimental results, however, for the overall probability of spin−orbit changing collisions. The disagreement is probably due at least in part to errors in the Ar−NO potential surface.

References and Notes

(1) Andresen, P.; Joswig, H.; Pauly, H.; Schinke, R. *J. Chem. Phys.* **1982**, *77*, 2204−2205.
(2) Joswig, H.; Andresen, P.; Schinke, R. *J. Chem. Phys.* **1986**, *85*, 1904−1914.
(3) Nielson, G. C.; Parker, G. A.; Pack, R. T. *J. Chem. Phys.* **1977**, *66*, 1396−1401.
(4) Bontuyan, L. S.; Suits, A. G.; Houston, P. L.; Whitaker, B. J. *J. Phys. Chem.* **1993**, *97*, 6342−6350.
(5) Jons, S. D.; Shirley, J. E.; Vonk, M. T.; Giese, C. F.; Gentry, W. R. *J. Chem. Phys.* **1992**, *97*, 7831−7834.
(6) Jons, S. D.; Shirley, J. E.; Vonk, M. T.; Giese, C. F.; Gentry, W. R. *J. Chem. Phys.* **1996**, *105*, 5397−5407.
(7) Meyer, H. *J. Chem. Phys.* **1995**, *102*, 3151−3169.
(8) Bieler, C. R.; Sanov, A.; Reisler, H. Chem. Phys. Lett. **1995**, *235*, 175−182.
(9) van Leuken, J. J.; van Amerom, F. H. W.; Bulthuis, J.; Snijders, J. G.; Stolte, S. *J. Phys. Chem.* **1995**, *99*, 15573−15579.
(10) Drabbels, M.; Wodke, A. M.; Yang, M.; Alexander, M. H. *J. Phys. Chem. A* **1997**, *101*, 6463−6474.
(11) van Leuken, J. J.; Bulthuis, J.; Stolte, S.; Snijders, J. G. *Chem. Phys. Lett.* **1996**, *260*, 595−603.
(12) Yang, X.; Wodke, A. M. *J. Chem. Phys.* **1992**, *96*, 5123−5128.
(13) Islam, M.; Smith, I. W. M.; Wiebrecht, J. W. *J. Phys. Chem.* **1994**, *98*, 9285−9290.
(14) Islam, M.; Smith, I. W. M.; Wiebrecht, J. W. *J. Chem. Phys.* **1995**, *103*, 9676−9691.
(15) James, P. L.; Sims, I. R.; Smith, I. W. M. *Chem. Phys. Lett.* **1997**, *272*, 412−418.
(16) James, P. L.; Sims, I. R.; Smith, I. W. M.; Alexander, M. H.; Yang, M. *J. Chem. Phys.* **1998**, *109*, 3882−3897.
(17) Yang, M.; Alexander, M. H. *J. Chem. Phys.* **1995**, *103*, 6973−6983.

(18) Alexander, M. H. *J. Chem. Phys.* **1993**, *99*, 7725−7738.

(19) HIBRIDON is a package of programs for the time-independent quantum treatment of inelastic collisions and photodissociation written by M. H. Alexander, D. E. Manolopoulos, H.-J. Werner, and B. Follmeg, with contributions by P. F. Vohralik, D. Lemoine, G. Corey, B. Johnson, T. Orlikowski, A. Berning, A. Degli-Esposti, C. Rist, P. Dagdigian, B. Pouilly, G. van der Sanden, M. Yang, F. de Weerd, and S. Gregurick.

(20) Proch, D.; Trickl, T. *Rev. Sci. Instrum.* **1989**, *60*, 713−716.

(21) Adams, T. E.; Morrison, R. J. S.; Grant, E. R. *Rev. Sci. Instrum.* **1980**, *51*, 141−142.

(22) Alexander, M. H.; Andresen, P.; Bacis, R.; Bersohn, R.; Comes, F. J.; Dagdigian, P. J.; Dixon, R. N.; Field, R. W.; Flynn, G. W.; Gericke, K.-H.; Grant, E. R.; Howard, B. J.; Huber, J. R.; King, D. S.; Kinsey, J. L.; Kleinermanns, K.; Kuchitsu, K.; Luntz, A. C.; McCaffery, A. J.; Pouilly, B.; Reisler, H.; Rosenwaks, S.; Rothe, E. W.; Shapiro, M.; Simons, J. P.; Vasudev, R.; Wiesenfeld, J. R.; Wittig, C.; Zare, R. N. *J. Chem. Phys.* **1988**, *89*, 1749−1753.

(23) Orr-Ewing, A. J.; Zare, R. N. *Annu. Rev. Phys. Chem.* **1994**, *45*, 315−366.

(24) Alexander, M. H.; Dagdigian, P. J. *J. Chem. Phys.* **1977**, *66*, 4126−4132.

(25) Sonnenfroh, D. M.; Liu, K. *Chem. Phys. Lett*. **1991**, *176*, 183−190.

(26) Hutson, J. M.; Green, S. MOLSCAT computer code, version 14 1994, distributed by Collaborative Computational Project No. 6 of the Engineering and Physical Sciences Research Council (U.K.).

(27) Dagdigian, P. J. In *Inelastic Scattering II. Optical Methods*; Scoles, G., Ed.; Atomic and Molecular Beam Methods, Vol. I; Oxford University Press: New York, 1988.

(28) Naulin, C.; Costes, M.; Benseddik, A.; Dorthe, G. *Laser Chem.* **1988**, *8*, 283−302.

(29) McGuire, P.; Kouri, D. J. *J. Chem. Phys.* **1974**, *60*, 2488−2499.

(30) Alexander, M. H.; Manolopoulos, D. E. *J. Chem. Phys.* **1987**, *86*, 2044−2050.

(31) Manolopoulos, D. E. *J. Chem. Phys.* **1986**, *85*, 6425−6429.

(32) Alexander, M. H. *J. Chem. Phys.* **1982**, *76*, 5974−5989.

(33) Dagdigian, P. J.; Alexander, M. H.; Liu, K. *J. Chem. Phys.* **1989**, *91*, 839−848.

(34) Kovalenko, L. J.; Delos, J. B. *J. Chem. Phys.* **1997**, *107*, 5473−5487.